Laboratory x-ray characterization of a surface acoustic wave on GaAs: critical role of the instrumental convolution

Ludovic Largeau, Ibrahima Camara, Jean-Yves Duquesne, Catherine Gourdon, Pauline Rovillain, L. Thevenard, Bernard Croset

Laboratory x-ray characterization of a surface acoustic wave on GaAs: critical role of the instrumental convolution.

Ludovic Largeau,[a] Ibrahima Camara,[b] Jean-Yves Duquesne,[b] Catherine Gourdon,[b] Pauline Rovillain,[b] Laura Thevenard[b] and Bernard Croset [b]*

[a]*Centre de Nanosciences et de Nanotechnologies, CNRS, Univ. Paris-Sud, Université Paris-Saclay, 91460, Marcoussis, France, and* [b]*Sorbonne Universités, UPMC Univ. Paris 06, CNRS-UMR 7588, Institut des Nanosciences de Paris, 75005, Paris, France. E-mail: bernard.croset@insp.jussieu.fr*

Abstract

Surface acoustic waves (SAW) of μm wavelength on a monocrystal give diffraction satellites around each Bragg peak in an x-ray diffraction diagram. By using a four crystal monochromator, a secondary two-crystal analyzer and masks reducing the fingerprint to the part of the crystal containing the acoustic modulation, their observation on a GaAS (001) surface is possible on a laboratory diffractometer. The finite extension of the satellites diffraction rods and of the crystal truncation rod perpendicularly to the surface leads to geometrical correction factors when convoluted with the instrumental resolution function which had previously been ignored. The calculations of these geometrical correction factors in the framework of the kinematic approximation allows

the determination of the surface acoustic wave amplitude and to study its attenuation and its dependence with RF power and duty cycle. The ability to perform such determinations with a laboratory diffractometer should prove useful to optimize SAWs which are presently used in a broad range of condensed matter physics studies.

1. Introduction

Since the pioneering work of Hauer & Burns (1975) an important effort has been devoted to studying the interactions between acoustic waves and x-rays (see *e.g.* Entin *et al.*, 1990, Roshchupkin & Brunel, 1992, Tucoulou *et al.*, 1997, Tucoulou *et al.*, 1998, Zolotoyabko & Polykarpov, 1998, Sauer *et al.*, 1999, Tucoulou *et al.*, 2001, Roshchupkin *et al.*, 2011, Bojahr *et al.*, 2012). One of the main motivations of these works has been the tailoring of synchrotron light. For this reason and because of the synchrotron high brilliance, most of the recent studies have been performed using synchrotron facilities. Tucoulou *et al.* (2001) showed that a surface acoustic wave of some ten micrometers wavelength propagating on a $LiNbO_3$ crystal leads to diffraction satellite peaks around each Bragg peak in a rocking curve. The q-separation between satellites being some thousandths of nm^{-1}, the very close proximity of the satellites to the Bragg peak implies the use of both a high resolution diffractometer and a good quality monocrystal. While these authors analyzed their results in the framework of kinematic theory of diffraction, some posterior works were analyzed thanks to dynamic theory (Schelokov *et al.*, 2004, Tucoulou *et al.*, 2005).

In the meantime, the interest for surface acoustic waves has known an increasing development. Excited electrically using interdigitated transducers (IDTs), they are routinely used as finite response filters in RF microelectronics up to 3 GHz. In more academic environments, they have recently emerged as an efficient tool for carrier and spin control in semiconductor and metallic nanostructures, with applications fore-

seen in quantum information technology (Sanada *et al.*, 2011, Hermelin *et al.*, 2011). Their versatility and the wide possibilities to tailor their interaction with electronic or magnetic excitations by using the toolbox of wave mechanics (interferences, focusing, wavefront and pulse shaping, etc.) make SAWs appealing to a growing number of condensed matter physicists (Li *et al.*, 2014, Schulein *et al.*, 2015, Thevenard *et al.*, 2016). Due to this active development of surface acoustic wave studies, there is a real need for an easy and versatile method to quantify their amplitude in view of optimizing the IDT design. This has been done in the past using optical light diffraction or interferometry (Lean *et al.*, 1970, Royer & Dieulesaint, 2001). We show here on a pristine GaAs substrate that this can also be performed using x-rays on a laboratory diffractometer through a careful experimental procedure and an adequate data analysis.

2. Experimental set-up and procedure.

2.1. Experimental set-up.

High resolution x-ray diffraction (HRXRD) measurements were carried out on a PANalytical X'pert Pro diffractometer equipped with a sealed Cu tube and in a triple axis geometry. A primary four-crystal Ge(220) monochromator and a secondary two-crystal Ge(220) analyzer were used. Such a geometry allows to select the Cu $K_{\alpha 1}$ radiation with $\lambda_{RX} = 0.1540562$ nm.

Using the piezoelectric properties of GaAs, we deposited two interdigitated transducer parallel to the <110> direction of an epiready substrate. The first IDT, IDT$_e$, allows the excitation of an acoustic wave propagating perpendicularly to this direction. The second IDT, was deposited $l_{gap} = 3$ mm to its left (Fig. 1). This is the standard SAW filter configuration which allows an electrical monitoring of the transmitted SAW shape (Royer & Dieulesaint, 2001). In this work, we have explored instead the right side of the IDT$_e$ using x-rays. The period of the IDT fingers was nominally $\lambda_a = 5\,\mu$m,

the metallization ratio, 0.5, the aperture, $W = 2\,\mathrm{mm}$ and the number of IDT finger pairs, $N = 60$. The electrodes were made of Cr/Au of nominal thickness 10/100 nm. The excitation signal is brought to the interdigital transducers by means of coaxial cables and coplanar waveguides with straight round bond-wires. Unless specified, the radio-frequency (RF) power is applied continuously (CW SAW mode). Otherwise it is modulated at low frequency by a square-wave of period $T_{mod} = 20\,\mu\mathrm{s}$ (Mod SAW mode). The resonance frequency of the IDT_e is measured to be $548 \pm 3\,\mathrm{MHz}$.

The acoustic waves propagation has been measured in-operando by collecting rocking curves and reciprocal space mappings (RSM). The crossed slits did not allow to define a sharp x-ray probe. Therefore, the use of masks for x-rays was required to limit the diffraction to the part of the crystal containing the acoustic modulation. We have placed glass masks with a $s_y = 2\,\mathrm{mm}$ width gap just above the surface while not being in contact in order not to disturb the acoustic waves propagation. The spot size was $s_x = 1.8$ mm for the (002) reflection and $s_x = 0.9$ mm for the (004) reflection. The center of the spot was positioned at a distance ranging from $x = 0$ to 7 mm to the right of the IDT_e (Fig. 1). Great care was taken to avoid any strain when attaching the sample to the holder.

2.2. Experimental procedure.

The x-ray spot was first positioned at $x = 2.1\,\mathrm{mm}$ from the IDT_e. The latter was excited at its resonance frequency with RF incoming powers ranging from $P_{elec} = 40\,\mathrm{mW}$ to $P_{elec} = 320\,\mathrm{mW}$. Figures 2, 3, 7, and 9 exhibit rocking curves around the (002) and the (004) Bragg peaks of the GaAs substrate. The presence of the acoustic wave leads to satellite features around the Bragg peaks. In order to carefully check that no thermal drift appears on the diffraction patterns when applying the electrical power on the IDT, we also excited it off its resonance, at 570 MHz. Diffraction patterns

identical to the one without any RF excitation were then recovered.

At the IDT resonance, the propagation of a SAW induces a sinusoidal modulation of the crystal in the propagation direction. Therefore, we expect diffraction satellites around each Bragg peak at positions given by $\mathbf{Q} = \mathbf{Q}_B + p\mathbf{q}_a$ where p is the satellite order, and $q_a = 2\pi/\lambda_a = 1.26\,10^{-3}\,\mathrm{nm}^{-1}$ is the acoustic wave vector and $\lambda_a = 5$ μm. The in-plane and the normal component of $\mathbf{Q}$ are given by $Q_{//} = 2\pi/\lambda_{RX}\,[\cos(2\theta - \omega) - \cos(\omega)]$ and $Q_z = -2\pi/\lambda_{RX}\,[\sin(2\theta - \omega) + \sin(\omega)]$. The angular positions of the satellites are then given by $1/\lambda_{RX}\,[\cos(2\theta_p - \omega_p) - \cos(\omega_p) - \cos(2\theta_B - \omega_B) + \cos(\omega_B)] = p/\lambda_a$ and $1/\lambda_{RX}\,[\sin(2\theta_p - \omega_p) - \sin(\omega_p) - \sin(2\theta_B - \omega_B) + \sin(\omega_B)] = 0$. Since the satellites appear for such low values of $\delta\omega = \omega - \omega_B$ of some hundredth of a degree, the components of $\mathbf{Q}$ for symmetric reflexions are simplified by $Q_{//} = Q_B/2\,[\delta(2\theta - \omega) - \delta(\omega)]$ and $Q_z = Q_B(1 + \cot(\theta)/2\,[\delta(2\theta - \omega) + \delta(\omega)])$. Therefore, the rocking curves are equivalent to $Q_{//}$-scans and $(\omega/2\theta,\, \omega)$ intensity maps are equivalent to $(Q_{//},\, \delta Q_z)$ intensity maps. A rapid analysis of the (002) $Q_{//}$-scans (Fig. 2) shows that, as expected, the satellite features are symmetric around the Bragg position, periodic with a period almost equal to the nominal acoustic wave-vector and that their intensities increase with the incoming RF power. These conclusions are less clear for the (004) $Q_{//}$-scans (Fig. 3) since the satellite features are not so well separated but once again the diffuse intensities outside the Bragg condition increase with the incoming RF power. Figure 4a exhibits a $(\omega/2\theta,\, \omega)$ intensity map around the (002) Bragg peak in presence of the acoustic wave. Satellites rods parallel to the Q_z-direction clearly appear. It is important to note that the extension of these rods in the Q_z-direction varies with the satellite order. In the next two sections, we will describe how to perform a quantitative analysis of these experimental features in order to extract the acoustic wave amplitude and to study its physical behavior as a function of different parameters : incoming RF power, distance to the IDT$_e$, SAW duty cycle (ratio of the "on" time to the modulation

period).

3. Modeling and data reduction.

In order to obtain a good estimate of the x-ray diffracted intensity, the first step is to get an accurate description of the atomic displacements associated with the surface acoustic wave traveling in the crystal. It is important to note that for a wavelength of the order of 5 μm, harmonic displacements of the order of 0.05 nm lead to a strain of the order of $6\,10^{-5}$. For such a small strain, the acoustic branch of the phonons can be calculated in the framework of linear elasticity of continuous media. In the case of cubic symmetry, for a (001) surface and a propagation in the <110> direction, the surface acoustic mode is a Rayleigh mode and one obtains for atomic displacements (Royer & Dieulesaint, 2001):

$$\begin{aligned} \mathbf{u}(x,y,z) &= \begin{pmatrix} u_x \\ u_y \\ u_z \end{pmatrix} = \begin{pmatrix} U_x(z)\cos(q_a x - \omega_a t) \\ 0 \\ U_z(z)\sin(q_a x - \omega_a t) \end{pmatrix} \\ &= \begin{pmatrix} 2U\exp(-p_r q_a z)\cos(p_i q_a z + \phi/2)\cos(q_a x - \omega_a t) \\ 0 \\ 2rU\exp(-p_r q_a z)\sin(p_i q_a z + \phi/2 - \psi)\sin(q_a x - \omega_a t) \end{pmatrix} \end{aligned} \tag{1}$$

where $q_a = 2\pi/\lambda_a$ and ω_a are the wave vector modulus and the angular frequency of the SAW, and r, p_r, p_i, ϕ, ψ are coefficients which depend on the elastic constants but are independent of the wave amplitude U. For GaAs using $C_{11} = 118.4\,\mathrm{GPa}$, $C_{12} = 53.7\,\mathrm{GPa}$, $C_{44} = 59.1\,\mathrm{GPa}$ (Cottam & Saunders 2001), one obtains $r = 1.34$, $p_r = 0.5$, $p_i = -0.48$, $\phi = -2.10$, $\psi = 2.61$, so that the surface atomic x and z displacement amplitudes at $z = 0$ are simply obtained as a function of U by: $u_x(z = 0)$=$0.99\,U$ and $u_z(z = 0)$=$-1.33\,U$. It is worth noting that i) the expression of $\mathbf{u}$ differs noticeably from a simple exponential damping used by previous authors (Tucoulou *et al.*, 2001), ii) a calculation performed in the framework of elasticity of continuous media implicitly assumes that all the atoms of the crystallographic unit cell have the same displacement.

Since the sound velocity, $v_a = \omega_a/q_a$, is much lower than the light velocity, the acoustic strain can be considered as quasi-static (Tucoulou *et al.*, 2001). Using the description of the atomic displacements, we can evaluate the amplitude $A(\mathbf{Q})$ of the x-ray diffracted wave in the framework of a kinematic approximation. The principle of the calculation has been developed by Tucoulou *et al.* (2001), based on earlier work of Entin *et al.* (1990). For a semi-infinite crystal $A(\mathbf{Q})$ can be written :

$$\begin{aligned} A(\mathbf{Q}) \propto \quad & F(\mathbf{Q}) \sum_{n_x=-\infty}^{\infty} \sum_{n_y=-\infty}^{\infty} \sum_{n_z=0}^{\infty} && [\exp(-\widetilde{\mu} R_z) \exp(i\mathbf{Q}\cdot\mathbf{R})] \\ \propto \quad & F(\mathbf{Q}) \sum_{n_x=-\infty}^{\infty} \sum_{n_y=-\infty}^{\infty} \sum_{n_z=0}^{\infty} && [\exp(-\widetilde{\mu} R_z) \exp(i\mathbf{Q}\cdot[\mathbf{R}_0+\mathbf{u}])] \\ \propto \quad & F(\mathbf{Q}) \sum_{G_y} \delta(Q_y - G_y) \sum_{n_x=-\infty}^{\infty} \sum_{n_z=0}^{\infty} && [\exp(-\widetilde{\mu} n_z a_z) \\ & && \exp(i[Q_x n_x a_x + Q_z n_z a_z]) \\ & && \exp(i[Q_x U_x(n_z a_z)\cos(q_a n_x a_x)]) \\ & && \exp(i[Q_z U_z(n_z a_z)\sin(q_a n_x a_x)])\,] \end{aligned} \tag{2}$$

where $F(\mathbf{Q})$ is the structure factor of the elementary mesh, δ is the Dirac distribution, G_y is the y-component of a reciprocal lattice node $\mathbf{G}$ and $\widetilde{\mu} = 1/2\,\mu_{GaAs}(1/\sin(\omega) + 1/\sin(2\theta-\omega))$ is the effective absorption coefficient for the x-ray amplitude. The $1/2$ factor accounts for the fact that μ_{GaAs}, the standard absorption coefficient, is defined with respect to the diffracted x-ray intensity (not amplitude), the importance of which will appear in the following since the satellite intensities are controlled by a subtle balance between x-ray absorption and acoustic wave amplitude decrease.

Defining $\rho_{\mathbf{Q}}(n_z a_z)$ and $\zeta_{\mathbf{Q}}(n_z a_z)$ by $\rho_{\mathbf{Q}}\sin(\zeta_{\mathbf{Q}}) = U_x Q_x$ and $\rho_{\mathbf{Q}}\cos(\zeta_{\mathbf{Q}}) = U_z Q_z$, $A(\mathbf{Q})$ yields:

$$\begin{aligned} A(\mathbf{Q}) \propto \quad & F(\mathbf{Q}) \sum_{G_y} \delta(Q_y - G_y) \sum_{n_x=-\infty}^{\infty} \sum_{n_z=0}^{\infty} && [\exp(-\widetilde{\mu} n_z a_z) \exp(i[Q_x n_x a_x + Q_z n_z a_z]) \\ & && \exp(i[\rho_{\mathbf{Q}}(n_z a_z)\sin(q_a n_x a_x + \zeta_{\mathbf{Q}}(n_z a_z))])\,] \end{aligned} \tag{3}$$

Using the identity $\exp(it\sin\theta) = \sum_{p=-\infty}^{\infty} J_p(t)\exp(ip\theta)$, $A(\mathbf{Q})$ can be written:

$$A(\mathbf{Q}) \propto F(\mathbf{Q}) \sum_{\mathbf{G}_{//}} \sum_{p=-\infty}^{\infty} \delta(\mathbf{Q}_{//} + p\mathbf{q}_a - \mathbf{G}_{//}) \sum_{n_z=0}^{\infty} \exp(iQ_z n_z a_z)\exp(-\widetilde{\mu} n_z a_z) J_p[\rho_{\mathbf{Q}}(n_z a_z)] \exp[i\zeta_{\mathbf{Q}}(n_z a_z)] \tag{4}$$

Since we have $q_a a_z \ll 1$, the dependence on n_z of $\rho_{\mathbf{Q}}$ and $\zeta_{\mathbf{Q}}$ is slow. Identically, we have $\widetilde{\mu} a_z \ll 1$ and the dependence on n_z of $\exp(-\widetilde{\mu} n_z a_z)$ is slow. Therefore, for each rod, satellite rod or crystal truncation rod, $A(\mathbf{Q})$ has strong maxima around each Bragg value G_z of Q_z. For the calculation of these maxima profiles, the summation on n_z can be substituted by an integral, leading to

$$A(\mathbf{Q}) \propto F(\mathbf{Q}) \sum_{\mathbf{G}} \sum_{p=-\infty}^{\infty} \delta(\mathbf{Q}_{//} + p\mathbf{q}_a - \mathbf{G}_{//}) H_{p,\mathbf{G}}(Q_z - G_z) \tag{5}$$

with

$$H_{p,\mathbf{G}}(q_z) = \int_0^{\infty} \exp(iq_z z)\exp(-\widetilde{\mu} z) J_p[\rho_{\mathbf{G}}(z)] \exp[i\zeta_{\mathbf{G}}(z)] dz \tag{6}$$

This expression shows that every Bragg peak is decorated by satellites in the q_x direction at positions $p\mathbf{q}_a$. While Bragg peaks and satellites have a δ-profile in the $\mathbf{Q}_{//} = (Q_x, Q_y)$ plane, their extension and their profile in the Q_z direction is controlled both by the finite penetration of the x-rays due to absorption and by the finite extension of the Rayleigh mode in the z direction. For simplicity's sake we will consider in the following, the case where $Q_x = 0$ but the conclusions are valid in the general case. For $Q_x = 0$, we have $\zeta = 0$ and $\rho = 2rUQ\exp(-p_r q_a z)\sin(p_i q_a z + \phi/2 - \psi)$. Since near $t = 0$ we have $J_0(t) = 1 + O(t^2)$ and $J_p(t) = O(t^p)$, the integrand factor in H behaves like $\exp(-[\widetilde{\mu} + p\, p_r q_a]z) = \exp(-[\widetilde{\mu} + p\mu_a]z)$ for large z with $\mu_a = 0.63\,\mu\mathrm{m}^{-1}$. From the NIST Standard Reference Database 126 (http://www.nist.gov/pml/data/xraycoef/) we have $\mu_{GaAs} = 0.039\,\mu\mathrm{m}^{-1}$ leading to $\widetilde{\mu}_{002} = 0.14\,\mu\mathrm{m}^{-1}$ and $\widetilde{\mu}_{004} = 0.067\,\mu\mathrm{m}^{-1}$. For small $U\,Q$, the asymptotic behavior of the Bessel functions is reached for small

values of z and the q_z profile of the diffracted intensity is essentially Lorentzian with a width 1/2 $(\widetilde{\mu} + p\mu_a)$. The width of the q_z-profiles increases with p, the Bragg peak being significantly narrower particularly in the (004) case. For larger values of $U\,Q$, the oscillations of the Bessel function must be taken into account to precisely describe the q_z-profiles but the main behavior is kept as can be seen on the intensity map of Figure 4.

So far, we have calculated like others before us (Tucoulou *et al.*, 2001), the diffracted amplitude $A(\mathbf{Q})$ and the "natural" intensity $I_{nat} = A\,A^*$, in the q_x, q_y, q_z space. To obtain the effective intensity, I_{eff} , one must convolute the natural intensity with the "instrumental" resolution function. This function accounts for several sources of peak broadening: angular resolutions, monochromaticity of the x-ray beam, finite-size effects (fingerprint size, crystal defects....). The small ratio between q_a and Q, $q_a/Q_{002} = 55\ 10^{-6}$ and $q_a/Q_{004} = 27.6\ 10^{-6}$, has two consequences: first the resolution function can be taken as constant when exploring the intensity landscape around each Bragg peak, second, as already pointed out, for the symmetric diffraction conditions corresponding to the (002) peak and the (004) peak, ω-scans can be considered as q_x-scans. The first point has an important consequence: in a ω-scan, i.e. a q_x-scan, all the peaks, the Bragg peak and the satellites, have the same q_x-profile, $B(q_x)$, which corresponds to the section of the instrumental resolution function in the ω direction. This unicity of the profile is of major importance when determining the intensity of the peaks by least-square fits. The "theoretical" profile to be fitted can be written $\sum_{p=-P}^{P} b + I_{|p|}B([q_x - Q_{00l} - pq_a]/\Delta q_x)$ where Δq_x is the profile width. The number of parameters to be fitted for $2P$ satellites is therefore $P+5$: the $P+1$ peak intensities, b, Q_{00l}, q_a and Δq_x. This important constraint allows to determine very weak satellites intensities even when badly separated from each other (for instance for the (004) scan, Fig. 5). Good fits can be obtained with a Gaussian for B. We find $\lambda_a = 5.01 \pm 0.2\ \mu$m

around the (002) Brakk peak and $\lambda_a = 5.21 \pm 0.2$ μm around the (004) Brakk peak. It is of major importance to examine the consequences of the convolution in the q_z direction, i.e. the $\omega - 2\theta$ direction. As pointed out before, the natural width in the q_z direction rapidly varies from peak to peak while the resolution function remains constant. Therefore, the result of the convolution leads to geometrical correction factors, $GCF = I_{eff}/I_{nat}$ which depend on the satellite order. These factors are of similar to the corrections for surface X-ray diffraction measurements (Vlieg, 1997, Robach *et al.*, 2000). We have not found in the literature devoted to the x-ray diffraction study of acoustic waves propagating on GaAs (Sauer *et al.*, 1999), $LiNbO_3$ (Tucoulou *et al.*, 2001), Si (Tucoulou *et al.*, 2000) or $La_3Ga_5SiO_{14}$ (Roshchupkin *et al.*, 2011) any example of calculation of such geometrical correction factors. Since the q_z-profile of each peak depends on U, the convolution and the calculation of the geometrical correction factors must be performed for each value of U. An example of such a convolution is given on Figure 4b. In order to calculate the geometrical correction factors, we have measured the instrumental resolution function without SAW, assuming that the profiles of the (002) and (004) Bragg peaks are controlled by the instrumental resolution function. For simplicity's sake, we assumed that these profiles are Gaussian, $B(q_x, q_z) \propto \exp(-[(q_x/\Delta q_x)^2) + (q_z/\Delta q_z)^2])$. We find: $\Delta q_x(002) = 4.1\,10^{-4}\,\mathrm{nm}^{-1}$, $\Delta q_z(002) = 15\,10^{-4}\,\mathrm{nm}^{-1}$, $\Delta q_x(004) = 6.7\,10^{-4}\,\mathrm{nm}^{-1}$ and $\Delta q_z(004) = 13\,10^{-4}\,\mathrm{nm}^{-1}$. We then performed numerically the convolution with the natural intensity by fast Fourier transform for several values of U with a 1 pm step. Table 1 illustrates the dependency of GCF with the peak order and the SAW amplitude. It is worth noting that the geometrical correction factors vary significantly with the peak order - half an order of magnitude when going from the Bragg peak to the satellites and 25% when going from first order to fourth order.

For each rocking-curve and each value of the incoming RF power, the peak intensities

are determined by least square fit. Then a second least square fit between measured and calculated effective intensities taking into account the geometrical correction factors allows the determination of U. Table 2 illustrates the result of this double fit procedure around the (002) Bragg peak for different incoming power.

When performing such a procedure, a difficulty occurs for the (004) rocking-curves: the kinematic approach we have chosen is not able to account for the intensity of the (004) Bragg peak while it accounts for the intensity of the satellites. This is due to the quite low value of $\widetilde{\mu}_{004}$. Therefore, we exclude the (004) Bragg peak of our analysis using solely the different satellites intensities. It is worth noting that previous authors have faced the same problem (Tucoulou *et al.*, 2001). This exclusion of the Bragg peak is compensated by the high number of satellites measurable around the (004) peak.

4. Data analysis.

Figure 6 exhibits the results obtained for U from rocking-scans around the (002) and (004) Bragg peaks as a function of the square root of the electric power. Two features appear clearly on this figure: first, the analyses around the (002) and (004) Bragg peaks lead to equivalent determinations of U, second the U values are proportional to the square root of the incoming RF power, as expected from the expressions of the acoustic Poynting vector (Royer & Dieulesaint, 2001). For the maximum CW power used (320 mW), the parameter $U = 0.083$ nm implies surface x and z displacements of $u_x(z=0) = 0.08$ nm and $u_z(z=0) = 0.11$ nm. Those correspond to surface strains $\epsilon_{xx} = 9.9\,10^{-5}$, $\epsilon_{xz} = 0$, $\epsilon_{zz} = 4.5\,10^{-5}$, (absolute values). Moreover, the acoustic power is then 2.44 W/m and the electro-mechanical conversion efficiency of the IDT_e is -18 dB. These are very decent values for SAWs excited directly on GaAs, without the addition of a traditionally more efficient piezoelectric material such as $LiNbO_3$ or ZnO.

This validation of our data reduction procedure allows laboratory studies of two physical questions:

- Using x-rays the absolute attenuation of the Rayleigh mode with the distance from the IDT_e can be determined. Figures 7 and 8 illustrate this study. For distances larger than to $x = 2\,\mathrm{mm}$ from the IDT_e, we find the Rayleigh mode to be exponentially damped with an attenuation coefficient of $5.9\,\mathrm{dB.cm^{-1}}$, reasonably lower than the one measured at 1 GHz by Slobodnik (1972). We also find the SAW amplitude to be identical on either side of the IDT_e, proving that no spurious reflexions off the receiving IDT lead to destructive interferences of the wave amplitude.
- The important relative variations of the satellite peaks with the Rayleigh mode amplitude allow to study it as a function of Mod SAW duty cycles, when modulating the RF power. We performed rocking-curves around the (002) Bragg peaks for several duty cycles of constant period, $T_{mod} = 20\,\mu\mathrm{s}$ and of variable "on" time, T_{on}. This implies that whereas the *average* displacement should decrease for weaker duty-cycles, the instantaneous displacement seen when the SAW is "on" should be identical. As shown in the two first columns of Table 3, for each duty cycle labelled by the ratio $\tau = T_{on}/T_{mod}$, we can satisfactorily fit the rocking-curve by a linear combination of the rocking-curves obtained for the two extreme conditions, $\tau = 0$ and $\tau = 1$. Figure 10 illustrates the quality of the fit obtained with such a linear combination. This result opens the road to a determination of the acoustic amplitude using non continuous wave excitation. For this determination, the Bragg peak must be excluded since its intensity depends on the ratio τ, but the relative satellite intensities are the same for any τ since they are only due to the times during which the incoming power is "on". The third column of Table 3 exhibits the acoustic wave amplitude, U, measured using

the first three satellites around the (002) Bragg peak. A study of the CW SAW allows to verify that the determination of U using the three satellites plus the Bragg peak leads to the same result as the determination with the sole three satellites. This possibility to determine U under Mod SAW is important since it allows to use high electric power for which a continuous wave excitation would damage the transducers.

5. Discussion and conclusion.

While a strict justification of our kinematic approach would imply a dynamic calculation, the overall results we obtained - good agreement between the values of U determined around the (002) and the (004) Bragg peaks, exponential decay of U with the distance from the IDT_e, determination of a constant U for variable duty cycle - validate our kinematic approach. This approach is based on four main points: i) good resolution in the q_x direction, $\Delta q_x \approx 5\,10^{-4}\,\mathrm{nm}^{-1}$, obtained using a four-crystal monochromator and a two-crystal analyzer; ii) reduction of the footprint to the crystal region affected by the acoustic wave using adequate masks; iii) calculation of the Rayleigh mode in the framework of linear elasticity of continuous media; iv) taking into account "geometrical" corrections due to finite instrumental resolution in the q_z direction, $\Delta q_z \approx 10^{-3}\,\mathrm{nm}^{-1}$.

It is worth noting that the determination of U implies measurements of quite low satellite intensities in the immediate vicinity of the Bragg Peak, for example $I_3/I_0 = 10^{-3}$ for $U = 0.05\,\mathrm{nm}$ around (002) and $I_6/I_0 = 2\,10^{-4}$ for $U = 0.036\,\mathrm{nm}$ around (004). These low values hinder a strict statistical estimate of the errors. Nevertheless, a study of the least square dependency on U allows to estimate $\Delta U/U$ to be of the order of 0.06. The exponential damping of the SAW leads to a relative variation of ± 0.07 for U in the 2 mm width of the x-ray spot around the (002) Bragg peak. This variation

is quite similar to our statistical incertainity and allows to neglect the damping in the data modeling that we have performed. Lastly, the measure of U depends on the correctness of the expression chosen for the acoustic mode. A minute error on the IDT orientation with respect to <110> will lead to a modification of expression (1), the acoustic wave no longer being a Rayleigh mode but a pseudo Rayleigh mode. A quantitative analysis of such an effect is far beyond the scope of this paper.

To conclude, we show that using both a careful experimental procedure and an accurate data analysis including instrumental convolution, measurements of surface acoustic wave amplitude can be performed on a laboratory x-ray diffractometer, provided the SAW spatial frequency is such that $q_a > \Delta q_x/2$. This work was performed on a GaAs monocrystal. However, since the satellite features appear in the in-plane direction, this diffraction technique can be applied to determine acoustic amplitudes in thin strained films. The ability to perform such determinations with a laboratory diffractometer is important given the versatility of experimental work performed using surface acoustic waves.

Acknowledgements We thank Christophe Rafaillac and Chris Lelong for the realization of the sample holder adapted to the RF cables, Loïc Beccera for the realization of the IDTs and Jean-Yves Prieur for fruitful discussions and advice. This work has been supported by the French Agence Nationale de la Recherche (ANR13-JS04- 0001-01).

References

Bojahr, A., Herzog, M., Schick, D., Vrejoiu, I. & Bargheer, M. (2012). *Phys. Rev. B* **86** 144306.

Cottam, R.I. & Saunders, G.A. (1973). *J. of Phys. C : Sol. State Phys.* **6**, 2105

Entin, I.R., Khrupa V.I. & Datsenko, L.I. (1990). *J. Appl. Cryst.* **23**, 355.

Hermelin, S., Takada, S., Yamamoto, M., Tarucha, S., Wieck, A.D., Saminadayar, L., Baüerle, C. & Meunier, T. (2011). *Nature* **477**, 435.

Hauer, R. & Burns, D.J. (1975). *Appl. Phys. Lett.* **27**, 524.

Lean, E.G.H. & Powell, C.G. (1972). *Proc. IEEE* **93**, **58** 1939 (1972)

Li, W., Buford, B., Jander, A. & Dhagat, P. (2014). *Physica B: Cond. Matt.* **448**, 151.

Robach, O., Garreau, Y., Aïd, K. & Véron-Jolliot, M.B. (2000). *J. Appl. Cryst.* **33**, 1006.

Roshchupkin, D.V. & Brunel, M. (1992). *Rev. Sci. Inst.* **64**, 379.

Roshchupkin, D.V., Irzhak, D., Snigirev, A., Snigireva, I., Ortega, L. & Sergeev, A. (2011). *J. Appl. Phys.* **110**, 124902.

Royer, D. & Dieulesaint, E. (2001). *Elastic waves in solids.* Heidelberg: Springer

Sanada, H., Sogawa, T., Gotoh, H., Onomitsu, K., Kohda, M., Nitta, J. & Santos, P.V. (2011). *Phys. Rev. Lett.* **106**, 216602.

Sauer, W., Streibl, M., Metzger, T.H., Haubrich, A.G.C., Manus, S., Wixforth, A. & Peisl, J. (1999). *Appl. Phys. Lett.* **75**, 639.

Schelokov, I.A., Roshchupkin, D.V., Irzhak, D.V. & Tucoulou, R. (2004). *J. Appl. Cryst.* **37**, 52.

Schülein, F.J.R., Zallo, E., Atkinson, P., Schmidt, O.G., Trotta, R., Rastelli, A., Wixforth, A. & Krenner, H.J. (2015). *Nature Nanotechnology* **10**, 512

Slobodnik, A.J. (1972). *Electronics Letters*, **8** 307

Thevenard, L., Camara, I.S., Majrab, S., Bernard, M., Rovillain, P., Lemaître, A., Gourdon, C. & Duquesne, J.-Y. (2016). *Phys. Rev. B* **93**, 134430 and *Phys. Rev. B* **93**, 140405.

Tucoulou, R., Roshchupkin, D.V., Schelokov, I.A., Brunel, M., Ortega, L. Ziegler, E., Lingham, M., Mouget, C. & Douillet, S. (1997). *Nucl. Instrum. Methods Phys. Res. B* **132**, 207.

Tucoulou, R., Roshchupkin, D.V., Mathon, O., Schelokov I.A., Brunel, M., Ziegler, E. & Morawe, C. (1998). *J. Synch. Rad.* **5**, 1357.

Tucoulou, R., Pascal, R., Brunel, M., Mathon,O., Roshchupkin, D.V., Schelokov, I.A., Cattan, E. & Remiens, D. (2000). *J. Appl. Cryst.* **33**, 1019.

Tucoulou, R., de Bergevin, F., Mathon, O. & Roshchupkin, D. (2001). *Phys. Rev. B* **64**, 134108.

Tucoulou, R., Mathon O., Ferrero, C., Mocella, V., Roshchupkin, D.V. & Kumon, R.E. (2005). *J. Appl. Phys.* **97**, 113505.

Vlieg, E. (1997). *J. Appl. Cryst.* **30**, 532.

Zolotoyabko, E. & Polikarpov, I. (1998). *J. Appl. Cryst.* **31**, 60.

Table 1. *Values of GCF, the geometrical correction factor, for different satellite orders around the (002) Bragg peak as function of U.*

U (pm)	GCF_0	GCF_1	GCF_2	GCF_3	GCF_4
23	0.142	0.639	0.708	0.767	0.805
34	0.139	0.635	0.704	0.766	0.804
62	0.135	0.621	0.690	0.758	0.799
86	0.146	0.614	0.671	0.746	0.792

Table 2. *Comparison between measured peak intensities, I_p, and best calculated peak intensities, C_p, around the* (002) *Bragg peak for various incoming powers.*

P	I_0	C_0	I_1	C_1	I_2	C_2	I_3	C_3	I_4	C_4
40	1	1	0.034	0.035	0.0011	0.00086	–	–	–	–
80	1	1	0.074	0.074	0.0044	0.0041	0.00062	0.00011	–	–
160	1	1	0.19	0.19	0.044	0.040	0.0056	0.0039	0.00075	0.00022
240	1	1	0.20	0.21	0.056	0.052	0.0089	0.0061	0.0012	0.00040
320	1	1	0.22	0.22	0.10	0.10	0.025	0.022	0.00039	0.0026

Table 3. *Determination of U using duty cycles.*
For each duty cycle, α corresponds to a fit by a linear combination of the 100% *and* 0% *rocking-curve, $(1-\alpha)\,I(\tau=0)+\alpha\,I(\tau=1)$. For the* 100% *duty cycle the value of U determined using the Bragg peak and the satellites is marked by a asterisk.*

$\tau = T_{on}/T_{tot}$	α	U (nm)
0.1	0.08 ± 0.07	0.057 ± 0.003
0.25	0.33 ± 0.07	0.051 ± 0.003
0.5	0.58 ± 0.07	0.051 ± 0.003
0.75	0.79 ± 0.07	0.050 ± 0.003
1	-	$0.054 \pm 0.003\,(0.053^*)$

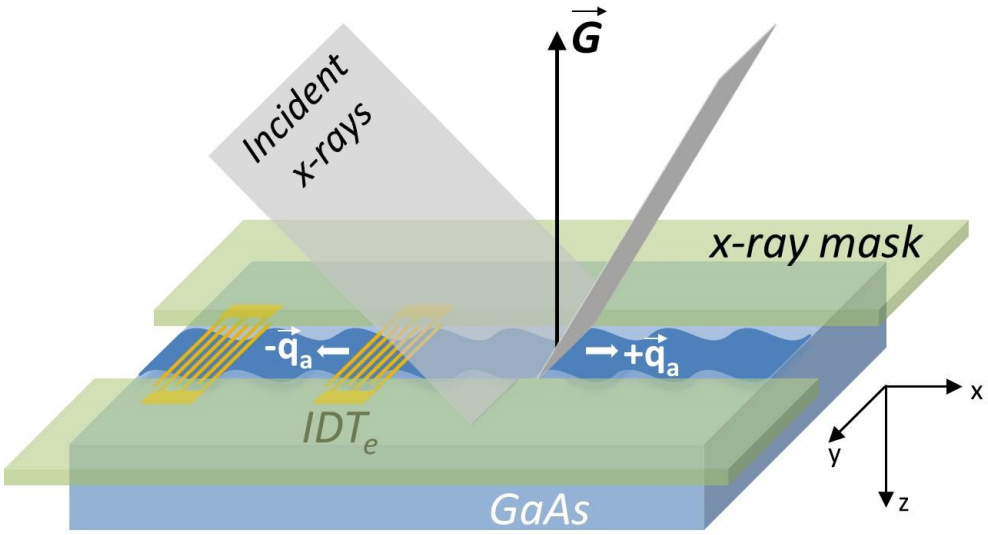

Fig. 1. Scheme of the experiment [not to scale]: the central metallic transducer (IDTe) deposited directly on GaAs emits bidirectionnaly a surface acoustic wave. The incident x-ray beam probes the induced displacement at different distances $x = 0 - 7$ mm. The glass masks ensure the x-rays are only scattered off the perturbed region of GaAs.

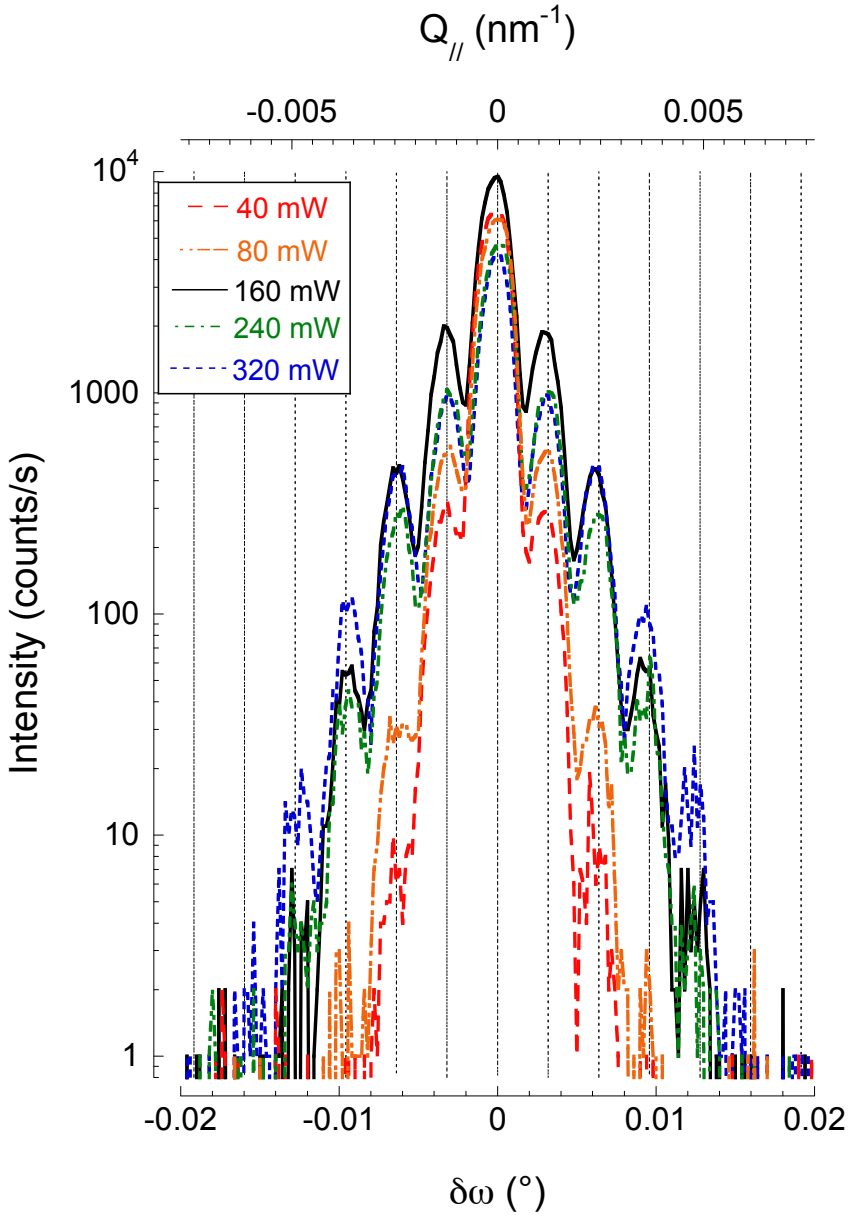

Fig. 2. Rocking curve around the (002) Bragg peak taken 2.1 mm from the IDT_e for increasing incoming RF power.
The vertical lines are guide for the eyes at $Q_{//} = \pm p\, q_a$.

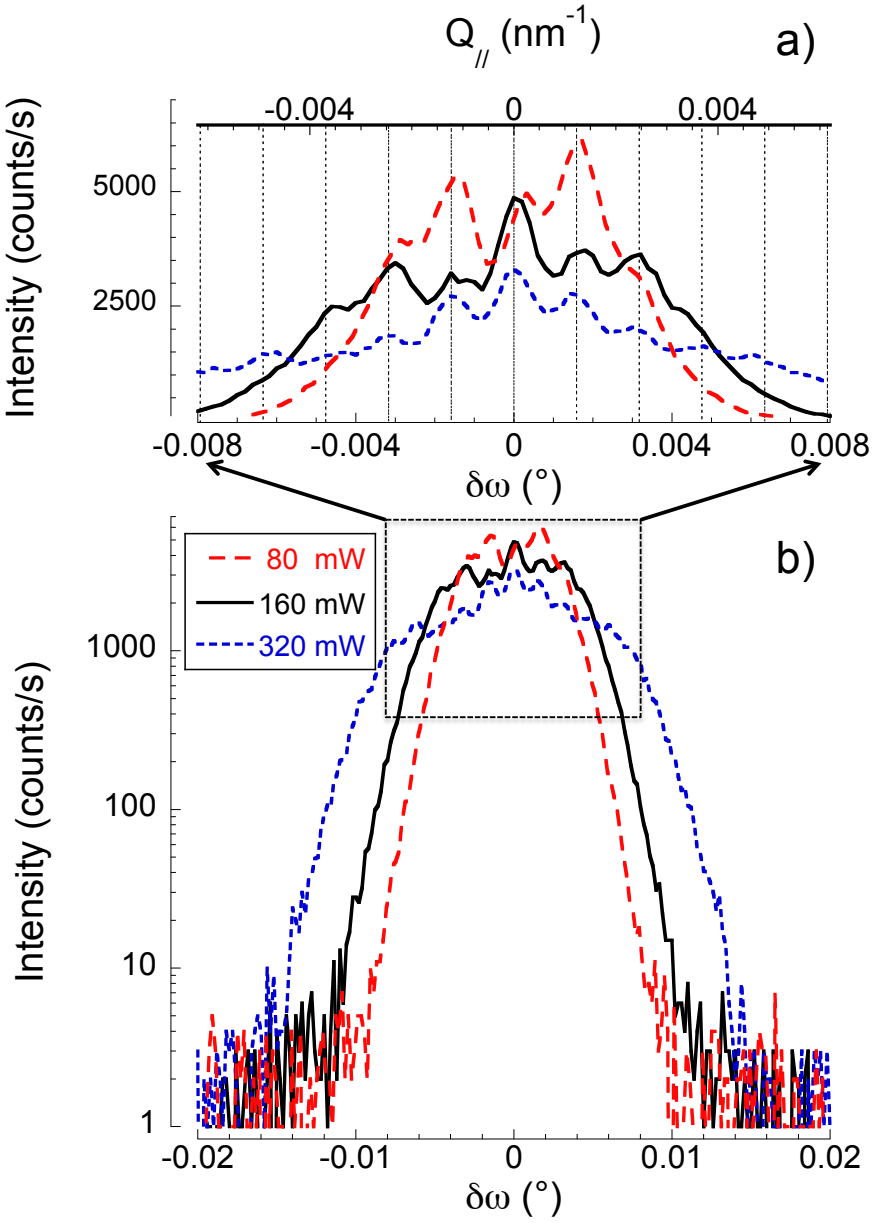

Fig. 3. Rocking curve around the (004) Bragg peak taken 2.1 mm from the IDT$_e$ for increasing incoming RF power.

a) Intensity in linear scale. The vertical lines are guide for the eyes at $Q_{//} = \pm p\, q_a$.

b) Intensity in logarithmic scale.

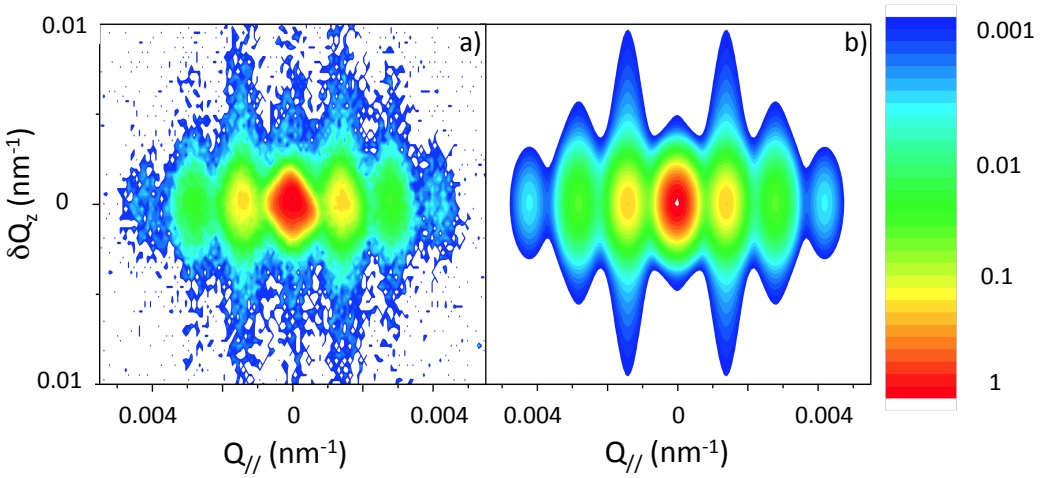

Fig. 4. Measured (a) and calculated (b) ($\omega/2\theta$, ω) intensity maps around the (002) Bragg peak ($x = 2.1\,\mathrm{mm}$, $P_{elec} = 160\,\mathrm{mW}$).

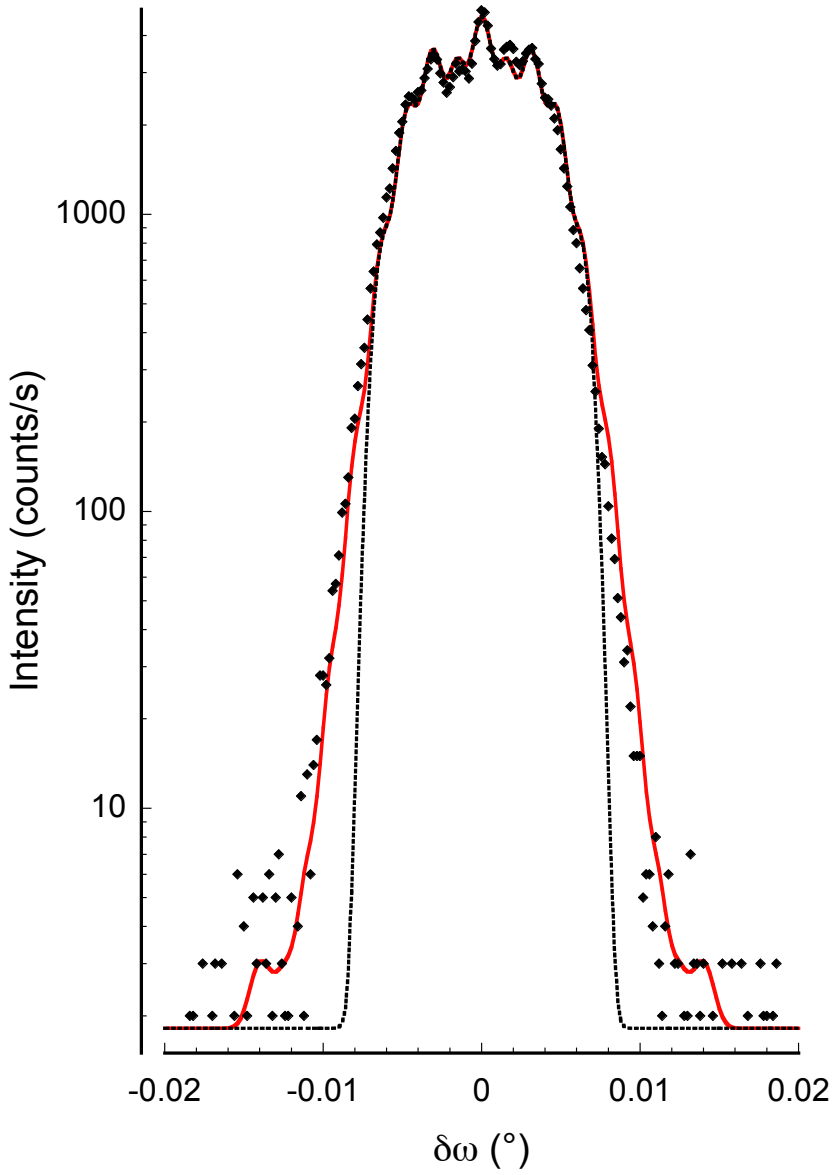

Fig. 5. Fit of the rocking curve around the (004) Bragg peak for an RF power of $P_{elec} = 160\,\mathrm{mW}$ ($x = 2.1\,\mathrm{mm}$). Black diamonds: observed intensity, red line: best fit with 2x8 Gaussian satellites and one central Gaussian, black dotted line: best fit with only 2x4 satellites and one central Gaussian.

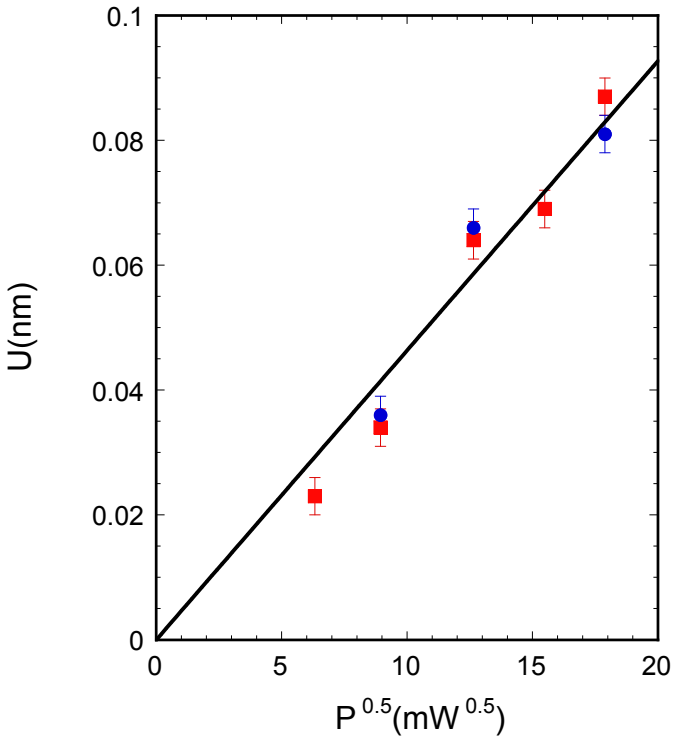

Fig. 6. Measured Rayleigh mode amplitude as a function of the square root of the incoming RF power.
Red square: (002) Bragg peak, Blue dots: (004) Bragg peak, Black line: Best fit by a proportional law $U = \gamma\, P^{0.5}$ leading to $\gamma = 4.6\,\mathrm{pm.mW^{-0.5}}$.

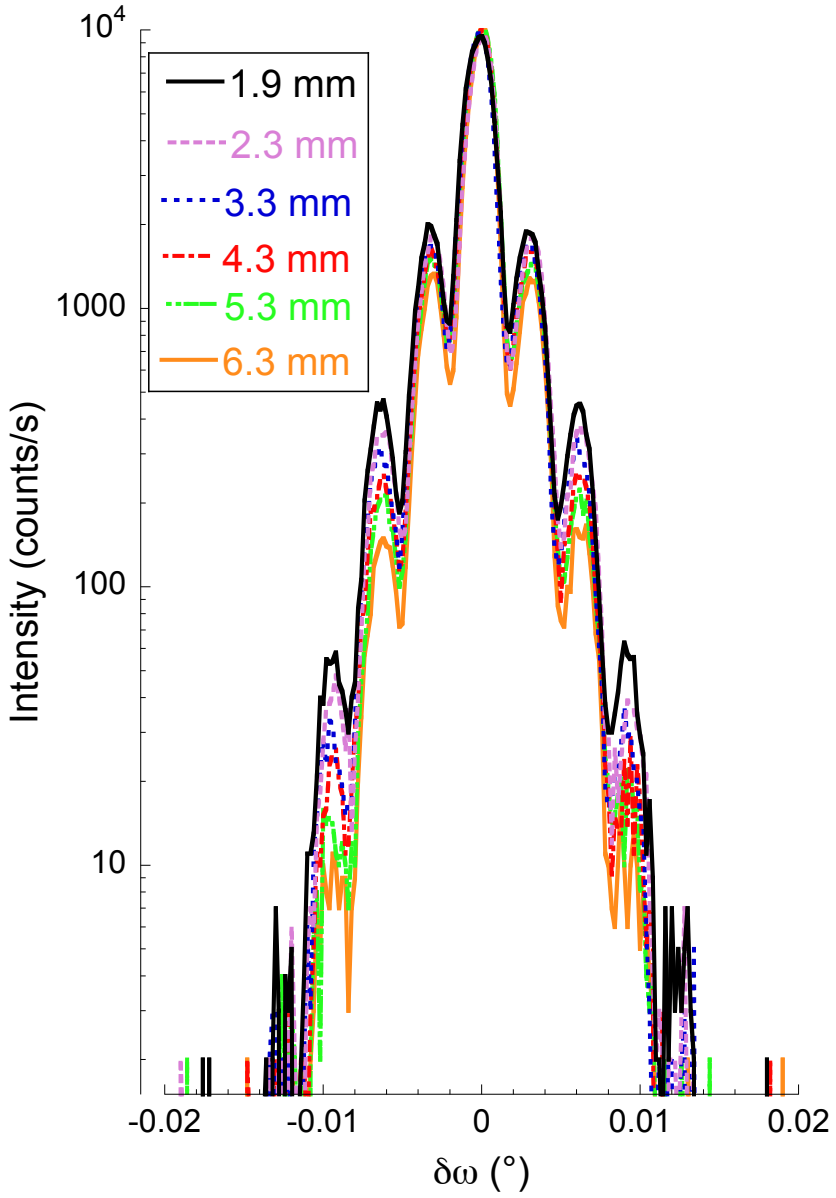

Fig. 7. Rocking curve around the (002) Bragg peak for increasing distances to the IDT$_e$ ($P_{elec} = 160$ mW).

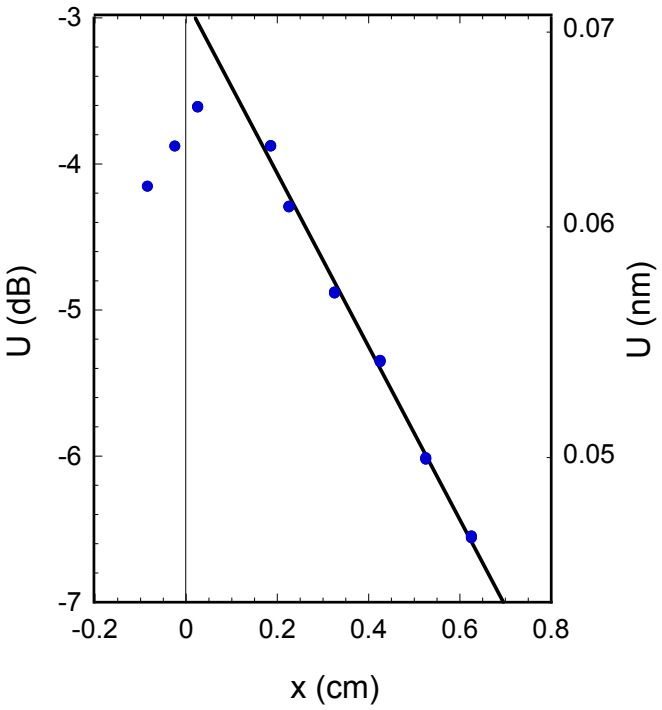

Fig. 8. Variation of the Rayleigh mode amplitude as a function of the distance to the IDT_e (P_{elec}=160 mW). Blue dots: Measured acoustic amplitude in dB (left axis) and its corresponding U value in nm (right axis in **log scale**), Black line: Exponential fit. The vertical black line materializes the right edge of the IDT_e.

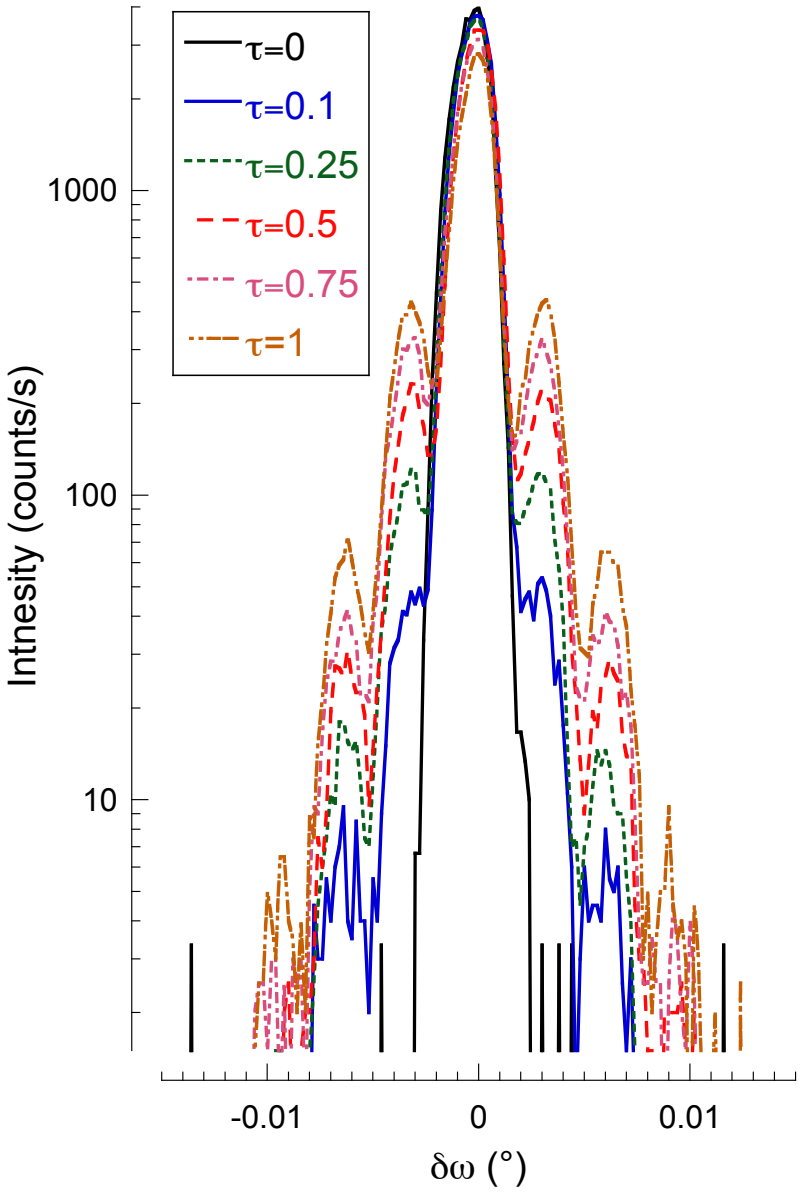

Fig. 9. Rocking curve around the (002) Bragg peak for duty cycles of constant period, $T_{mod} = 20\mu$s and of variable "on" time, $T_{on} = \tau\, T_{mod}$ ($x = 2.1$ mm, $P_{elec} = 160$ mW).

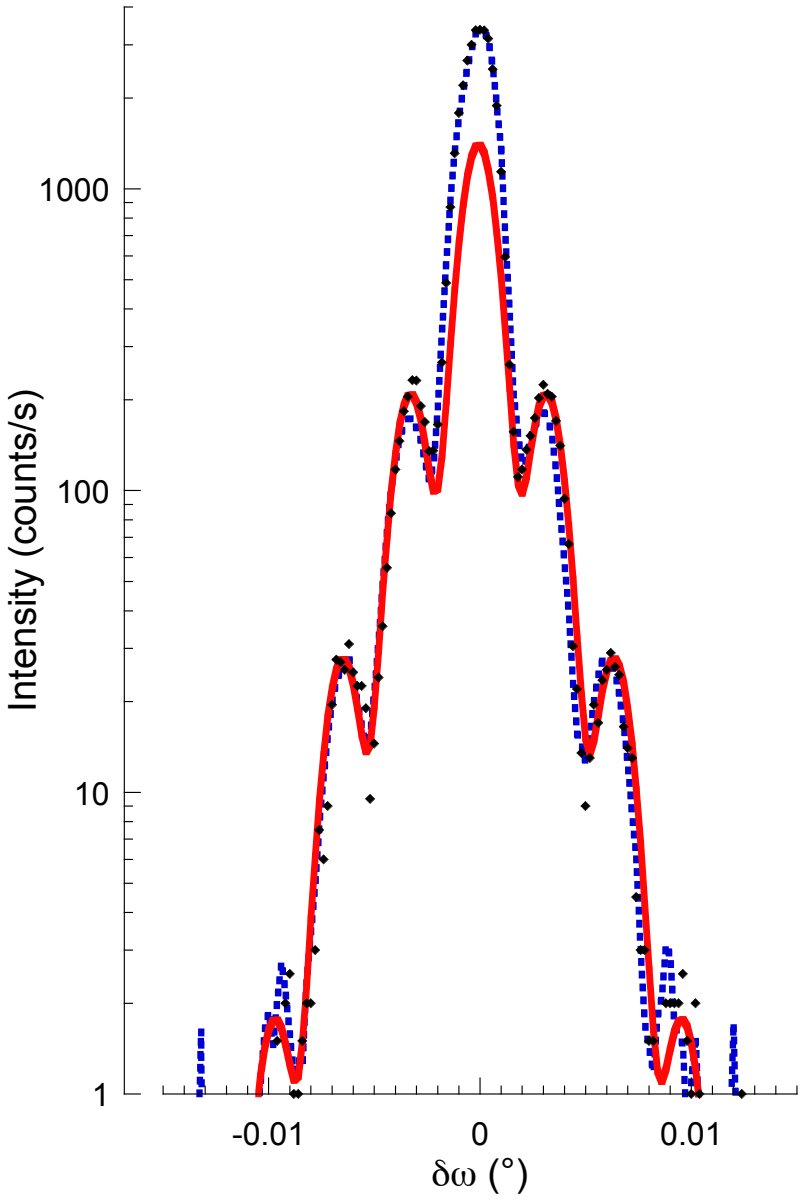

Fig. 10. Rocking-curve around the (002) Bragg peak for a duty-cycle of 50% ($x = 2.1$ mm, P_{elec}= 160 mW).
Black diamond: observed intensity, blue dotted line: best linear combination of 0% and 100% rocking curve, red full line: best calculated curve with a determination of U using the sole three satellites. (Note the discrepancy between the observed and the calculated curves near the Bragg peak.)

Synopsis

It is demonstrated that a measurement of a surface acoustic wave amplitude can be performed on a laboratory diffractometer through a careful experimental procedure and an adequate data analysis. The importance of the fingerprint reduction and of geometrical correction factors due to finite experimental resolution are emphasized.